Quantum Electronics **40** (1) 45 – 50 (2010)

NONLINEAR OPTICAL PHENOMENA

PACS numbers: 42.55.Fx; 42.70.Gi; 61.48.De
DOI: 10.1070/QE2010v040n01ABEH014163

Nonlinear light scattering in a carbon nanotube suspension

G.M. Mikheev, T.N. Mogileva, A.V. Okotrub, D.L. Bulatov, V.V. Vanyukov

***Abstract*. Nonlinear scattering of 1064-nm laser light in an aqueous suspension of purified carbon nanotubes has been studied in relation to their optical power limiting behaviour using *z*-scan measurements to simultaneously determine the energy and shape of the transmitted and 90°-scattered pulses. The results indicate that the reduction in transmitted laser pulse energy with increasing incident power density is mainly due to the associated increase in scattered pulse energy. The shape, duration and time shift of the transmitted and 90°-scattered pulses are intricate functions of incident power density. The data are interpreted in terms of thermally induced nonlinear and Rayleigh scattering processes at high and low incident power densities, respectively.**

Keywords: *optical power limiting, nonlinear scattering, pulse shape, z-scan measurements, laser radiation, carbon nanotube suspension.*

1. Introduction

The study of optical power limiting (OPL) in nanomaterials is of interest for the development of effective laser light optical limiters capable of protecting light-sensitive objects from high-power laser beams [1 – 4]. Suspensions of nanocarbon materials have attracted considerable attention because they can be used as broadband optical limiters [5, 6]. OPL in various materials and suspensions of carbon nanostructures has been the subject of extensive studies [7 – 13]. OPL experiments typically utilise the *z*-scan technique, in which the transmission of the system, e.g. a suspension in a cuvette, is measured as a function of its position relative to the laser beam waist [14] (see also Refs [3, 12, 15]). The transmittance of the cuvette may be influenced by nonlinear absorption, nonlinear refraction and nonlinear scattering. Probing the interaction zone with a low-power laser beam demonstrates that OPL in carbon nanotube (CNT) suspensions is due to nonlinear scattering by vapour bubbles that result from the transfer of the energy absorbed by the carbon material to the liquid, and also from carbon sublimation [2]. In spite of the many reports on OPL, no experiments aimed at correlating the reduction in transmission to the increase in scattered light intensity in *z*-scan measurements have been described in the literature. Also, there are no experimental data on the amplitude and temporal characteristics of the pulsed radiation resulting from nonlinear scattering in OPL materials. Given the above, the purpose of this paper was to study the characteristics of the light pulses resulting from the nonlinear scattering of laser radiation in OPL systems as exemplified by an aqueous CNT suspension.

2. Preparation and characterisation of the suspension

We studied OPL in an aqueous suspension of multiwalled CNTs synthesised through arc-vaporisation of graphite [16, 17]. To ensure the formation of a stable nanotube suspension in water and remove glassy carbon nanoparticles from the nanotube surface, the sample was chemically treated as described elsewhere [18]. The oxidation of the multiwalled CNTs with a potassium permanganate solution in sulphuric acid produced oxygen-containing surface groups, which ensured the formation of a colloidal CNT solution in water [19]. The aqueous CNT suspension thus prepared was stable for a long time (more than a year). Examination of the nanoparticles on a JEOL JSM-6700F scanning electron microscope (SEM) confirmed that the sample was free of amorphous carbon and glassy carbon particles. At the same time, the sample contained few or no long CNTs. Most of

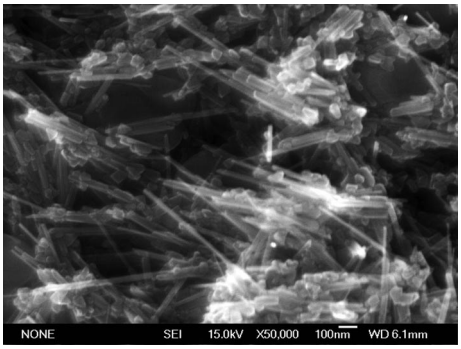

Figure 1. SEM micrograph of nanoparticles in the suspension.

G.M. Mikheev, T.N. Mogileva, D.L. Bulatov, V.V. Vanyukov
Institute of Applied Mechanics, Ural Branch, Russian Academy of Sciences, ul. T. Baramzinoi 34, 426067 Izhevsk, Russia;
e-mail: mikheev@udman.ru;
A.V. Okotrub Nikolaev Institute of Inorganic Chemistry, Siberian Branch, Russian Academy of Sciences, prosp. Akademika Lavrent'eva 3, 630090 Novosibirsk, Russia

Received 4 June 2009; revision received 10 November 2009
Kvantovaya Elektronika **40** (1) 45 – 50 (2010)
Translated by O.M. Tsarev

the particles were 15–20 nm in diameter and less than 1 μm in length (Fig. 1).

3. Measurement technique

In our experiments, we used an automated laser system ($\lambda = 1064$ nm; pulse repetition rate, 1 Hz; pulse duration, $\tau = 17 \pm 1$ ns [20]). The initial transmittance T_0 of the suspension, enclosed in a 1-mm-thick glass cuvette, was 45% at 1064 nm. OPL was studied using z-scan measurements, schematically illustrated in Fig. 2. The setup differs fundamentally from known configurations in that the light sensor in position (*1*) and the cuvette containing the suspension (*2*) are mounted directly on the positioning stage (*3*) so that, in the course of z-scan measurements, the active area of the sensor is always opposite to the lateral side of the cuvette. This allowed us to monitor the energy, amplitude and temporal characteristics of the 90°-scattered laser light while moving the cuvette along the optical axis z, with the origin at the laser beam waist. The focal length of the collecting lens was 100 mm, and the beam waist diameter was $2r_0 = 100$ μm. The incident and transmitted laser pulses were detected by sensors placed on the optical axis in positions (*4*) and (*5*).

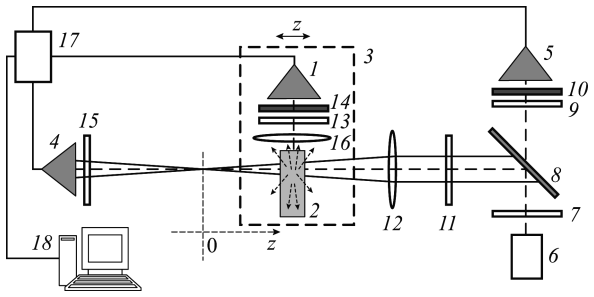

Figure 2. Experimental arrangement for modernised z-scan measurements: (*1*, *4*, *5*) positions of light sensors; (*2*) cuvette filled with the suspension; (*3*) positioning stage; (*6*) laser source; (*7*, *13*) IKS optical filters; (*8*) semi-transparent mirror; (*9*, *11*, *15*) neutral filters; (*10*, *14*) ground glass; (*12*) collecting lens; (*16*) collimating lens; (*17*) multichannel laser pulse energy measurement system; (*18*) computer.

The sensors used to monitor the energy characteristics of the incident, transmitted and scattered pulses were FD-24 photodiodes, incorporated into the multichannel laser pulse energy measurement system [20]. The pulse energies at the input (ε_{in}) and output (ε_{out}) of the measurement section comprising the collecting lens and optical cuvette were used to determine the transmittance of the cuvette filled with the suspension, $T = (\varepsilon_{out}/\varepsilon_{in})100$ %, as a function of the distance z from the cuvette to the focus ($z = 0$) of the collecting lens. Measuring the 90°-scattered laser pulse energy, ε_s (relative units), synchronously with the transmitted energy, we were able to assess the nonlinear-scattering contribution to the reduction in T with increasing incident power density (decreasing $|z|$).

When the amplitude and temporal characteristics of the incident, transmitted and scattered pulses were measured, the end faces of two optical fibres of different lengths, with a core diameter of 200 μm, were used in place of sensors (*1*) and (*4*) [or (*5*)]. The output ends of the fibres were coupled to the input of a Thorlabs SIR5-FC high-speed photodetector, having a rise time less than 70 ps. Photoelectric pulses were visualised using a Tektronix 7704B 7-GHz digital oscilloscope, having an input resistance of 50 Ω. After each laser pulse, the oscilloscope display showed two electrical pulses, the latter of which had a predetermined time delay. This allowed us to evaluate the temporal parameters of the incident, 90°-scattered and transmitted pulses. It should be noted that the fibres were selected so that they did not distort the shape of nanosecond pulses, which was verified experimentally. The digital oscilloscope allowed both a single pulse and the average over a particular number of laser shots to be examined. When averages were taken over ten or more laser pulses, the stable system of oscilloscope trigger with an avalanche photodiode, which recorded light leakage from the laser cavity, enabled examination of the pulse shape with a single sensor in the form of a short (0.6 m) fibre, whose end was placed successively in positions (*1*), (*4*) and (*5*) (Fig. 2).

4. Experimental results and discussion

Figure 3 shows the measured transmittance T and energy ε_s as functions of z for the suspension moved along the optical axis at $\varepsilon_{in} = 0.3$ mJ. As z approaches zero (the incident power density increases), the transmittance of the suspension, T, decreases markedly (Fig. 3a) and, accordingly, the

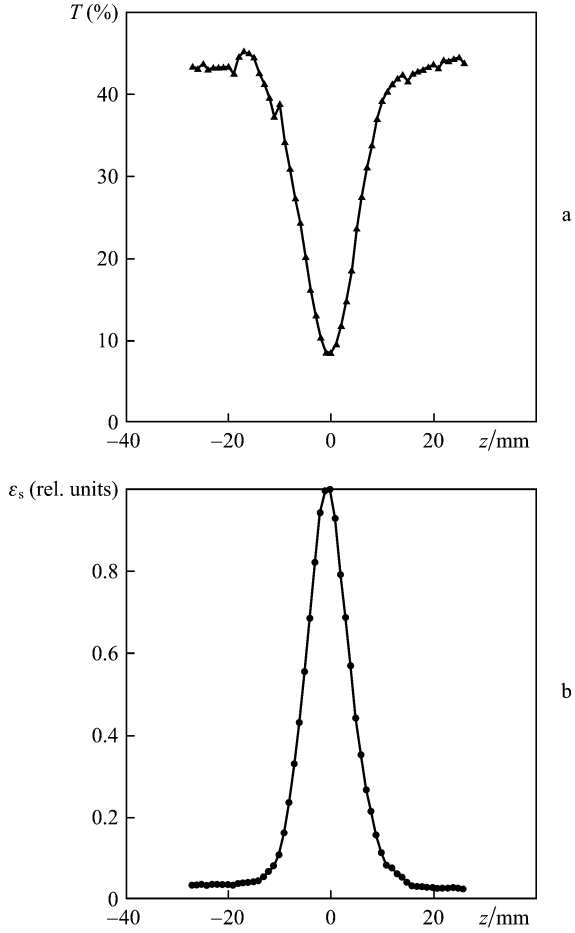

Figure 3. (a) Transmittance at the output of the cuvette filled with the suspension, T, and (b) 90°-scattered laser pulse energy, ε_s, as functions of z at $\varepsilon_{in} = 0.3$ mJ.

90°-scattered laser pulse energy, ε_s, increases, i.e., the higher the ε_s, the lower the transmittance T. Note that, away from the beam waist, the 90°-scattered laser light energy does not vanish, remaining roughly constant. Clearly, this is due to the Rayleigh scattering in the suspension, which is dependent on the nanoparticle concentration.

It is of interest to analyse the experimental data presented in Fig. 3. To this end, consider the energy balance for laser pulses incident on and transmitted through the cuvette when there is no OPL:

$$\varepsilon_{in} = \varepsilon_{out} + \varepsilon_{ab} + \varepsilon_r + \varepsilon_{Rs}, \quad (1)$$

where ε_{ab}, ε_r and ε_{Rs} are the energies absorbed in the suspension, reflected from the cuvette wall and scattered in all directions through the Rayleigh scattering from the nanoparticles, respectively. The initial transmittance of the cuvette filled with the suspension is then given by

$$T_0 = \frac{\varepsilon_{in} - \varepsilon_{ab} - \varepsilon_r - \varepsilon_{Rs}}{\varepsilon_{in}}. \quad (2)$$

Under the assumption that OPL is only due to nonlinear scattering, the transmittance obtained in a z-scan measurement can be written in the form

$$T = T_0 - \frac{\varepsilon_s^{4\pi}}{\varepsilon_{in}}, \quad (3)$$

where $\varepsilon_s^{4\pi}$ is the energy scattered through the full 4π solid angle, which depends on the incident power density (or on z). Clearly, the measured 90°-scattered pulse energy, ε_s (relative units), is proportional to ε_s. Consequently, the above relation can be rewritten in the form

$$T = T_0 - k\varepsilon_s, \quad (4)$$

where k is a proportionality factor.

Figure 4 presents the $T(\varepsilon_s)$ data points derived from the $T(z)$ and $\varepsilon_s(z)$ data in Fig. 3. For this purpose, the small pedestal due to Rayleigh scattering was subtracted from all the ε_s values. Lines (*1*) and (*2*) represent, respectively, linear and quadratic fits to the data. The linear fit is seen to poorly represent the experimental data, whereas the quadratic relation provides a good fit to the data points. Therefore, Eqn (4), though in qualitative agreement with the experimental data in Fig. 4, is insufficiently accurate. This in turn suggests that the OPL is due not only to nonlinear scattering but also to nonlinear laser light absorption, which is left out of account in (3). The nonlinear-absorption contribution to OPL can be estimated using the $T(z)$ and $\varepsilon_s(z)$ data in Fig. 3 represented as T and ε_s vs. incident power density, $I = \varepsilon_{in}/(\tau S)$. Here $S = \pi r^2$ is the cross-sectional area of the laser beam and r is the Gaussian beam radius, given by [21]

$$r(z) = r_0\left[1 + \left(\frac{\lambda z}{\pi r_0^2}\right)\right]^{1/2}, \quad (5)$$

where r_0 is the beam waist radius.

Taking into account the energy balance, we find that the contribution of nonlinear absorption to OPL is $\sim 10\,\%$ and, hence, it is not a dominant process. This result has important implications for understanding the nature of OPL in carbon nanoparticle suspensions.

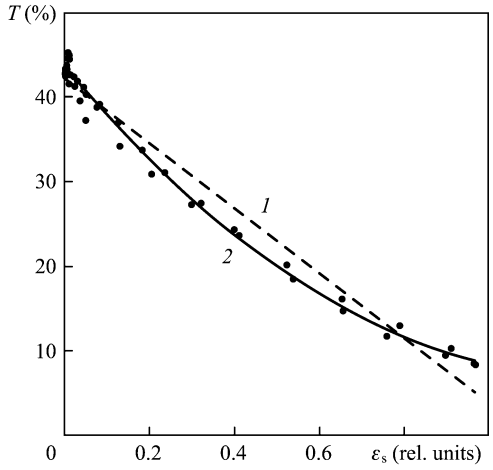

Figure 4. Transmittance T vs. 90°-scattered pulse energy ε_s. The data points are derived from the experimental data in Fig. 3. (*1*) linear fit; (*2*) quadratic fit.

Figure 5 shows the experimentally determined shapes of the incident (P_{in}), transmitted (P_{out}) and 90°-scattered (S_{90}) light pulses at $\varepsilon_{in} = 1.5$ mJ and various values of z. Note that curve (*1*) in Fig. 5a represents a laser pulse transmitted through the suspension with no OPL. For the convenience of time delay representation, the pulses in Fig. 5b are scaled to give a peak height of unity. Comparison of the data in Figs 3a and 5a leads us to conclude that the reduction in transmittance T with decreasing $|z|$ (increasing incident power density) is attributable to the reduction in the relative width of the transmitted (leading) part of the laser pulse: at a smaller $|z|$, a narrower part of the pulse passes through

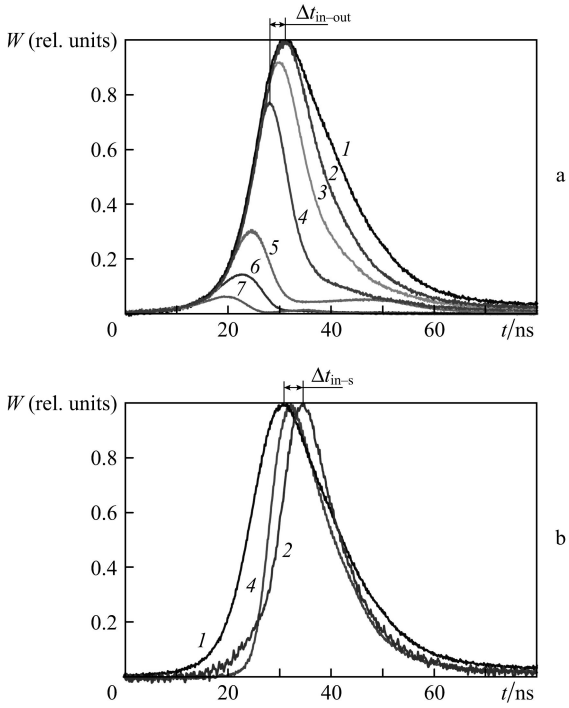

Figure 5. Shapes of the (a) transmitted and (b) 90°-scattered light pulses at $\varepsilon_{in} = 1.5$ mJ and $z = 32$ (*2*), 24 (*3*), 17 (*4*), 7 (*5*), 4 (*6*) and 0 mm (*7*); (*1*) shape of the incident laser pulse.

the suspension. Clearly, the rest (trailing part) of the pulse is either scattered or absorbed in the suspension. Therefore, the transmitted pulse peak leads the incident pulse peak, and the time delay $\Delta t_{\text{in-out}}$ between the peaks increases as the cuvette approaches the beam waist (Fig. 6). Note that the maximum $\Delta t_{\text{in-out}}$ value, which is reached at the beam waist, decreases with decreasing ε_{in} (Fig. 6).

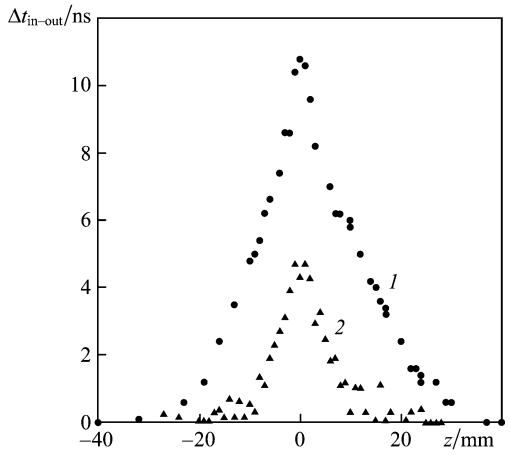

Figure 6. Time delay between the incident and transmitted pulse peaks, $\Delta t_{\text{in-out}}$, as a function of z at $\varepsilon_{\text{in}} = 1.5$ (*1*) and 0.3 mJ (*2*).

It should be stressed that the full width at half maximum (FWHM) of the transmitted laser pulse varies with z [Fig. 7, inset, curve (*1*)] and has a minimum when the cuvette is at the beam waist. The reduction in $\tau_{\text{hw}}^{\text{out}}$ is due to the fact that nonlinear scattering cuts off the trailing part of the pulse (Fig. 7). The 10 % – 90 % rise time of the transmitted pulse varies little [Fig. 7, inset, curve (*2*)], with a slight dip around $z = 0$. Comparison of the transmitted pulse shapes at various ε_{in} values (Figs 5a, 7) near the beam waist shows that, at a high input energy ($\varepsilon_{\text{in}} = 1.5$ mJ), the trailing part of the transmitted pulse has a pedestal with a poorly defined second peak [Fig. 5, curves (*5–7*)]. At $\varepsilon_{\text{in}} = 0.3$ mJ, there is no pedestal [Fig. 7, curves (*2–7*)]. This seems to be due to relaxation processes that occur in the zone where the high-power laser beam interacts with the suspension and depend on the incident power density. Detailed analysis of the transmitted pulse shape in relation to OPL is beyond the scope of the present paper.

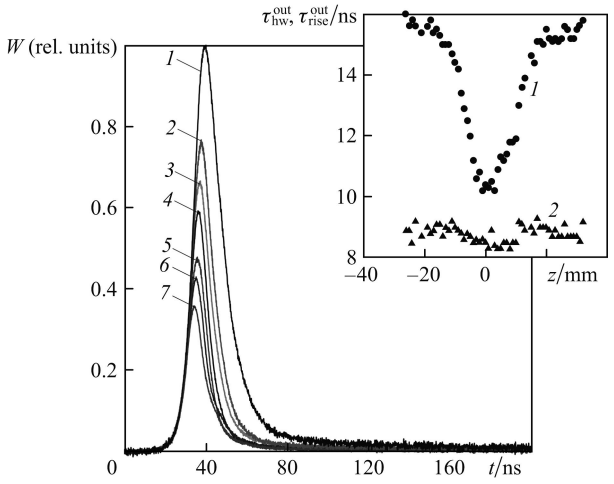

Figure 7. Shapes of (*1*) incident and (*2–7*) transmitted laser pulses; $z = 6$ (*2*), 5 (*3*), 4 (*4*), 2 (*5*), 1 (*6*), and 0 mm (*7*). Inset: (*1*) duration $\tau_{\text{hw}}^{\text{out}}$ and (*2*) rise time $\tau_{\text{rise}}^{\text{out}}$ of transmitted laser pulses as functions of z at $\varepsilon_{\text{in}} = 0.3$ mJ.

The experimental data in Fig. 5b, obtained at $\varepsilon_{\text{in}} = 1.5$ mJ, demonstrates that the 90°-scattered pulses differ markedly in shape from the transmitted pulses. When the cuvette filled with the suspension is away from the beam waist, e.g. at $z = 32$ mm, the peak of the S_{90} pulse, with a 13-ns duration, lags the P_{in} pulse peak by $\Delta t_{\text{in-s}} = 3.2$ ns [Fig. 5b, curve (*2*)]. At a pulse FWHM of 18 ns [Fig. 5b, curve (*1*)], the delay is quite significant. Thus, the scattered pulse due to the OPL in the suspension is in general narrower and its maximum lags that of the incident pulse, that is, the S_{90} pulse emerges and builds up with a time delay relative to the P_{in} pulse. All this points to a thermally induced nonlinear scattering mechanism.

Figure 8 plots the amplitude A, rise time $\tau_{\text{rise}}^{\text{s}}$, 90% – 10% fall time $\tau_{\text{fall}}^{\text{s}}$, FWHM $\tau_{\text{hw}}^{\text{s}}$ and delay time $\Delta t_{\text{in-s}}$ against z for the 90°-scattered pulse at an incident laser pulse energy $\varepsilon_{\text{in}} = 1.5$ mJ. At $z = 0$, i.e., when the cuvette filled with the suspension is at the beam waist, where the input power density has a maximum, the amplitude A also reaches a maximum [Fig. 8, curve (*1*)]. Away from the beam waist, the amplitude of the 90°-scattered pulse drops sharply. All this correlates with the large amount of data, obtained in this study (see e.g. Fig. 3a) and earlier (see e.g. Refs [3, 4]), on the variation of the transmission of carbon nanoparticle suspensions with z in OPL experiments. Indeed, such data demonstrate that, if a suspension exhibits OPL behaviour, its transmittance drops sharply as z approaches zero. Therefore, this sharp decrease in transmission is attributable to a

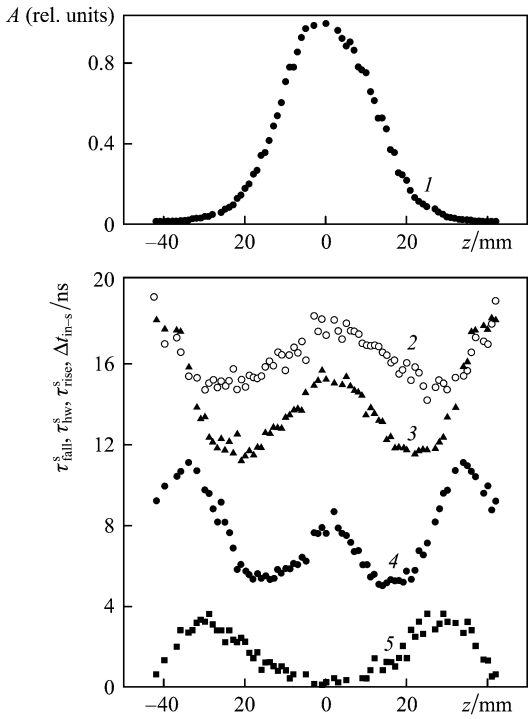

Figure 8. (*1*) Amplitude (A), (*2*) fall time ($\tau_{\text{fall}}^{\text{s}}$), (*3*) duration ($\tau_{\text{hw}}^{\text{s}}$), (*4*) rise time ($\tau_{\text{rise}}^{\text{s}}$) and (*5*) time delay relative to the incident pulse peak ($\Delta t_{\text{in-s}}$) as functions of z for the 90°-scattered pulse.

considerable increase in the conversion efficiency from the incident laser pulse power to the power scattered in all directions, including the normal to the z axis, as well illustrated by curve (*1*) in Fig. 8.

It also follows from Fig. 8 that the duration τ^{s}_{hw}, rise time τ^{s}_{rise} and fall time τ^{s}_{fall} of the 90°-scattered pulse depend significantly on z, with a maximum at $z = 0$. Increasing the magnitude of z (reducing the incident power density) gradually reduces τ^{s}_{hw}, to a minimum at $z_{opt} \sim \pm 23$ mm. At the same time, curve (*1*) in Fig. 8 shows that, at $z = \pm z_{opt}$, the S_{90} pulse amplitude is about one-tenth that at $z = 0$. As $|z|$ increases further, τ^{s}_{hw} rises, reaching the input pulse duration. The $\tau^{s}_{rise}(z)$ and $\tau^{s}_{fall}(z)$ curves also show non-monotonic behaviour.

No less interesting is the variation of Δt_{in-s} with z [Fig. 8, curve (*5*)]. In the vicinity of $z = 0$, there is no time delay between the incident and 90°-scattered pulses. With increasing $|z|$, Δt_{in-s} gradually rises. As seen in Fig. 8, the increase in Δt_{in-s} is accompanied by a reduction in the 90°-scattered pulse amplitude and duration. At $|z| \sim z_{cr}$ ($z_{cr} > z_{opt}$), Δt_{in-s} reaches a maximum, before gradually falling off to zero. Concurrently, the amplitude A becomes very small. Clearly, at large $|z|$, where the incident laser power density is low and no OPL occurs, the 90°-scattered pulse shape is determined by Rayleigh scattering and, accordingly, coincides with the input pulse shape. Therefore, Δt_{in-s} must approach zero at large $|z|$, and the scattered pulse parameters τ^{s}_{rise}, τ^{s}_{fall} and τ^{s}_{hw} must coincide with those of the incident laser pulse, as observed in experiment.

Similar measurements were made at other laser pulse energies. The curves obtained at different ε_{in} values are similar in shape, but at lower ε_{in} values the variations in A, τ^{s}_{rise}, τ^{s}_{fall}, τ^{s}_{hw} and Δt_{in-s} take place in narrower z ranges, which correlates with the experimental data in Fig. 6 and confirms that the characteristics of the scattered pulse depend on the incident power density, I.

The experimental data in Fig. 8 and relation (*5*) can be used to evaluate the scattered pulse parameters as functions of I (Figs 9, 10). As seen in Fig. 9, the scattered pulse amplitude follows a power law at low I (inset, solid curve). At high power densities, the $A(I)$ data can be fitted with a straight line in a relatively wide range. Given the above, it follows from Fig. 10 that the scattered pulse parameters τ^{s}_{rise}, τ^{s}_{fall}, τ^{s}_{hw} and Δt_{in-s} are intricate functions of incident power density. The time delayΔt_{in-s} has a maximum at $I \sim 60$ MW cm^{-2}, and the scattered pulse duration τ^{s}_{hw} has a minimum at $I \sim 100$ MW cm^{-2}, where it is about a factor of 1.5 shorter than the incident laser pulse duration.

All the present results on OPL in the CNT suspension are consistent with a thermally induced nonlinear scattering mechanism [2, 8], detailed discussion of which is beyond the scope of the present paper.

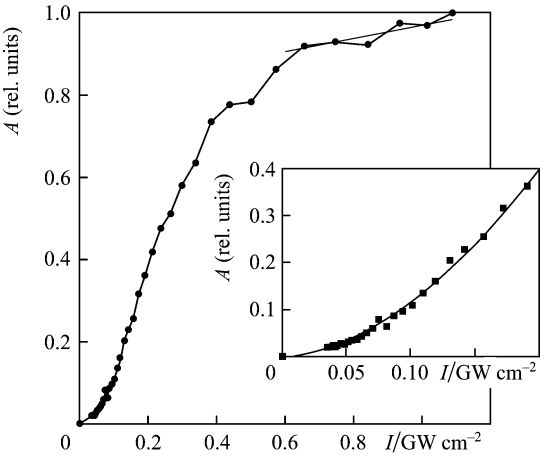

Figure 9. Scattered pulse amplitude A as a function of incident power density I. The straight line represents the least-squares fit to the data for $I > 600$ MW cm^{-2}. Inset: best-fit curve of the form $A = k_1 I + k_2 I^{1.8}$ for $I < 200$ MW cm^{-2}.

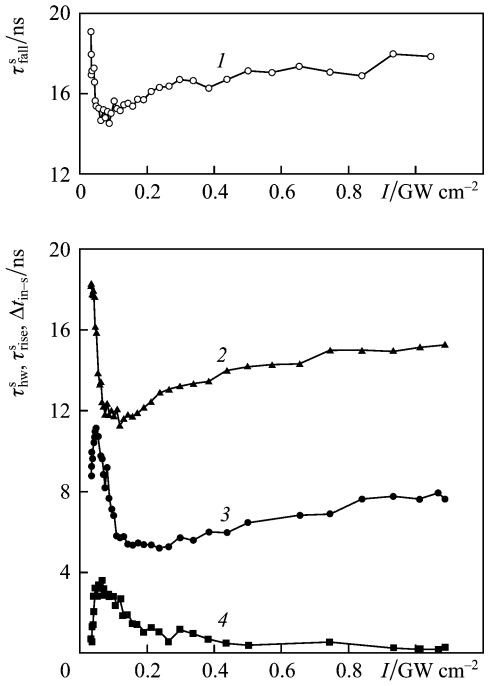

Figure 10. (*1*) Fall time τ^{s}_{fall}, (*2*) duration τ^{s}_{hw}, (*3*) rise time τ^{s}_{rise} and (*4*) time delay Δt_{in-s} as functions of incident power density I for the 90°-scattered pulse.

5. Conclusions

The results obtained here using a modernised z-scan technique indicate that OPL in aqueous CNT suspensions is mainly due to nonlinear scattering. The contribution of nonlinear absorption to OPL is much less significant ($\sim 10\,\%$). Our experimental data demonstrate that, in general, the transmitted pulse peak in an OPL system leads the incident pulse peak and that nonlinear scattering cuts off the trailing part of the pulse. The 90°-scattered pulse parameters (amplitude, duration, rise time, fall time, and time delay) are intricate functions of incident laser power density because of the transition from Rayleigh scattering at low incident intensities to thermally induced nonlinear scattering at high intensities.

Acknowledgements. This work was supported by the Siberian and Ural Branches of the Russian Academy of Sciences (Joint Research Project No. 102: Optoelectrical and Nonlinear Optical Properties of Carbon Nanotubes and Their Suspensions).

References

1. Mansour K., Soileau M.J., Van Stryland E.W. *J. Opt. Soc. Am. B.*, **9** (7), 1100 (1992).
2. Vivien L., Lançon P., Riehl D., Hache F., Anglaret E. *Carbon*, **40**, 1789 (2002).
3. Ganeev R.A., Kamanina N.V., Kulagin I.A., Ryasnyanskii A.I., Tugushev R.I., Usmanov T.B. *Kvantovaya Elektron.*, **32**, 781 (2002) [*Quantum Electron.*, **32**, 781 (2002)].
4. Mikheeva O.P., Sidorov A.I. *Pis'ma Zh. Tekh. Fiz.*, **30** (6), 16 (2004).
5. Sun X., Yu R.Q., Xu G.Q., Hor T.S.A., Ji W. *Appl. Phys. Lett.*, **73** (25), 3632 (1998).
6. Vivien L., Anglaret E., Riehl D., et. al. *Opt. Commun.*, **174**, 271 (2000).
7. Nashold K.M., Walter D.P. *J.Opt. Soc. Am. B*, **12** (7), 1228 (1995).
8. Mishra S.R., Rawat H.S., Mehendale S.C., et al. *Chem. Phys. Lett.*, **317**, 510 (2000).
9. Koudoumas E., Kokkinaki O., Konstantaki M., Couris S., Korovin S., Detkov P., Kuznetsov V., Pimenov S., Pustovoi V. *Chem. Phys. Lett.*, **357**, 336 (2002).
10. Chin K.C., Gohel A., Elim H.I., et al. *J. Mater. Res.*, **21**, 2758 (2006).
11. Mikheev G.M., Bulatov D.L., Mogileva T.N., et al. *Pis'ma Zh. Tekh. Fiz.*, **33** (6), 41 (2007).
12. Ganeev R.A., Usmanov T.B. *Kvantovaya Elektron.*, **37**, 605 (2007) [*Quantum Electron.*, **37**, 605 (2007)].
13. Mikheev G.M., Kuznetsov V.L., Bulatov D.L., et al. *Kvantovaya Elektron.*, **39**, 342 (2009) [*Quantum Electron.*, **39**, 342 (2009)].
14. Shiek-Bahae M., Said A.A., Van Stryland E.W. *Opt. Lett.*, **14**, 955 (1989).
15. Chunosova S.S., Svetlichnyi V.A., Meshalkin Yu.P. *Kvantovaya Elektron.*, **35** (5), 415 (2005) [*Quantum Electron.*, **35** (5), 415 (2005)].
16. Okotrub A.V., Shevtsov Yu.V., Nasonova L.I., et al. *Prib. Tekh. Eksp.*, **1**, 193 (1995).
17. Okotrub A.V., Bulusheva L.G., Romanenko A.I., et al. *Appl. Phys. A*, **21**, 481 (2001).
18. Okotrub A.V., Yudanov N.F., Aleksashin V.M., et al. *Vysokomol. Soedin., Ser. A*, **49**, 1049 (2007).
19. Bahr J.L., Tour J.M. *J. Mater. Chem.*, **12**, 1952 (2002).
20. Mikheev G.M., Mogileva T.N., Popov A.Yu., Kalyuzhnyi D.G. *Prib. Tekh. Eksp.*, **2**, 101 (2003).
21. Rykalin N.N., Uglov A.A., Zuev I.V., Kokora A.N. *Lazernaya i elektronno-luchevaya obrabotka materialov* (Laser and Electron Beam Processing of Materials) (Moscow: Mashinostroenie, 1985).